Magn Reson Mater Phy (2008) 21:149–158
DOI 10.1007/s10334-007-0101-3

RESEARCH ARTICLE

MR venography of the human brain using susceptibility weighted imaging at very high field strength

Peter J. Koopmans · Rashindra Manniesing · Wiro J. Niessen · Max A. Viergever · Markus Barth

Received: 9 July 2007 / Revised: 10 December 2007 / Accepted: 10 December 2007 / Published online: 11 January 2008

Abstract
Objective We investigate the implications of high magnetic field strength on MR venography based on susceptibility-weighted imaging (SWI) and estimate the optimum echo time to obtain maximum contrast between blood and brain tissue.
Materials and methods We measured tissue contrast and T_2^* relaxation times at 7 T of gray matter, white matter, and venous blood in vivo.
Results T_2^* relaxation times of gray matter, white matter, and venous blood in vivo yielded 32.9 ± 2.3, 27.7 ± 4.3, and 7.4 ± 1.4 ms, respectively. Optimum TE was found to be 15 ms which is supported by theoretical considerations. Using this optimum TE, we acquired 3D high resolution datasets with a large volume coverage in a short measurement time that show very detailed microanatomical structures of the human brain such as intracortical veins and laminar cortical substructures.
Conclusions By applying optimised vessel filters (vesselness filter and vessel enhancing diffusion) whole brain MR venograms can be obtained at 7 T with a significantly reduced measurement time compared to 3 T.

Keywords Neuroimaging · Venography · 3 T · 7 T · Parallel imaging · Vessel segmentation · Vessel enhancing diffusion · Transverse relaxation times

P. J. Koopmans · M. Barth (✉)
F.C. Donders Centre for Cognitive Neuroimaging,
Radboud University Nijmegen, P.O. Box 9101,
Nijmegen 6500 HB, The Netherlands
e-mail: markus.barth@fcdonders.ru.nl

R. Manniesing · W. J. Niessen
Department of Medical Informatics and Radiology,
Rotterdam, The Netherlands

M. A. Viergever
Image Sciences Institute, University Medical Center,
Utrecht, The Netherlands

M. Barth
Erwin L. Hahn Institute for Magnetic Resonance Imaging,
University Duisburg-Essen, Essen, Germany

Introduction

The purpose of this paper is to describe the implications of very high magnetic field strengths—namely 3 and 7 T—for the contrast of SWI-based MR venography [1]. SWI is based on the (static) blood oxygenation level dependent (BOLD) effect [2–5] and has primarily been used at a low field strength of 1.5 T. Within the recent years the applications of SWI have been extended well beyond MR venography. They range from clinical applications, such as tumor diagnostics [6–9], trauma [10], stroke [11], and multiple sclerosis [12], to applications in functional MRI to remove venous contributions [13]. High magnetic fields have potential advantages for SWI, due to higher intrinsic SNR but, more importantly, due to higher contrast in both magnitude and phase images for tissues that contain iron-carrying paramagnetic substances. One could think of deoxyhaemoglobin in venous structures, but also ferritin in deep brain nuclei or methemoglobin contained in certain neuropathologies.

However, when B_0 is changed it is important to optimise sequence parameters, in particular echo time TE, as T_2^* values change significantly with field strength. The important practical implications of high fields are: At first, maximum contrast between veins and surrounding tissue can be obtained at a shorter TE; thus, TR can be reduced resulting in shorter measurement times. Secondly, the net magnetization is higher, leading to a higher intrinsic signal that can

be traded off for higher spatial resolution or shorter measurement time, or both. In addition, shortening measurement times by using parallel imaging methods becomes more beneficial at high fields [14]. In the following: we estimate the echo time that is optimal for MR venography at high fields by investigating T_2^* related effects. We use these findings to acquire high resolution datasets with large volume coverage in a relatively short measurement time that show very detailed anatomical structures of the human brain down to laminar cortical substructures. Furthermore, by applying dedicated filters (Utrecht vesselness filter and vessel enhancing diffusion) detailed whole brain MR venograms can be obtained.

Theoretical considerations

SWI-based MR venography uses the fact that paramagnetic deoxyhaemoglobin in veins causes a shift in resonance frequency between the venous vessel and the surrounding tissue. This leads to dephasing in case both tissues are present within a voxel. A difference in T_2^* relaxation times of venous blood and brain tissues is another source of contrast [2]. In case the vein is not running parallel to B_0 an additional extravascular field around the vessel can also cause signal cancellation due to the induced magnetic field gradients in the extravascular space [15]. In gradient echo imaging the resulting signal loss can be large, which makes it possible to visualise even small, sub-voxel sized vessels due to these combined effects [1,3–5]. SWI-based venography does not require a sufficient flow velocity, as do other MR angiographic methods, which enables the depiction of very small venous vessels. In SWI-based venography, high spatial resolution increases the venous blood volume fraction within a voxel and leads to a better visualisation of small venous structures. High resolution comes at the cost of decreased SNR and longer measurement times which can, at least partly, be compensated for by using higher field strengths.

In order to estimate the echo time at which optimum contrast is obtained at different field strengths one can calculate pure T_2^* contrast C(TE) between venous blood and tissue according to:

$$C(TE) = \exp(-TE/T_{2T}^*) - \exp(-TE/T_{2B}^*) \quad (1)$$

Here, T_{2B}^* denotes the relaxation time of blood and T_{2T}^* denotes the one of tissue at the field strength of interest. We used the results of T_2^* measurements at 7 T that we performed in this study and used Eq. 1 to obtain the echo time for optimum contrast for MR venography at this field strength and experimentally validated this estimation.

Materials and methods

MR imaging

All experiments were performed on whole body MRI scanners (Siemens, Erlangen, Germany) at field strengths of 3 and 7 T. At 3 T the 8 channel head array of the manufacturer was used and, for imaging the visual cortex, a custom built eight channel array (Stark Contrast, MRI Coils, Erlangen, Germany) covering the occipital cortex (see [13]). At 7 T a CP head coil (InVivo, USA) and an eight channel array coil (RAPID, Germany) were used. Where indicated, parallel imaging implemented as GRAPPA [16] was used to accelerate the acquisition by an acceleration factor (AF) of 2.

SWI data were obtained using a 3D, first-order flow-compensated gradient echo FLASH sequence. The following imaging parameters were used:

3 T: repetition time (TR) = 35 ms, echo time (TE) = 28 ms, flip angle (α) = 15°, readout bandwidth (BW) = 120 Hz/px. For the occipital SWI dataset a resolution of 0.75 × 0.75 × 0.75 mm^3 (0.42 µl) was used (MA = 144 × 192; 40 slices). The original dataset had eight functional volumes (acquisition time TA = 2 min per volume) which were acquired using the occipital coil array. Only the "rest condition" volumes were used because functional activation reduces the contrast between dark veins and bright brain tissue in activated areas. For more details on this dataset see [13]. The whole brain SWI dataset (TA = 15 min, AF = 2, 128 slices) was acquired with a resolution of 0.57 × 0.57 × 1.25 mm^3 (0.41 µl) using a sagittal slab orientation to reduce artefacts related to turbulent flow in arteries near the base of the brain.

7 T: TR = 22 ms, TE = 15 ms, α = 15°, BW = 120 Hz/px. The whole brain SWI dataset (TA = 10 min, AF = 2, 128 slices) was acquired in sagittal orientation with a resolution of 0.57 × 0.57 × 1.25 mm^3 (0.41 µl). To detect very small anatomical structures a transverse orientation with a resolution of 0.27 × 0.27 × 1.5 mm^3 (109 nl) was used (TA = 13:30 min, AF = 2, 72 slices). In order to estimate T_2^*, a multi (twelve) echo version of the previously described sequence (without flow compensation) was used in four subjects with TE ranging from 5 ms to 60 ms (TR = 70 ms), interecho delay was 5 ms (BW 210 Hz/px). T_2^* values of gray matter (GM), white matter (WM) and venous blood were obtained using respective ROIs from a non-linear fit routine (curvefit) implemented in IDL (Creaso, Germany). All echoes were used in the fit procedure except for estimating the short T_2^* of venous blood in the sagittal sinus where the first five echoes were used. By using ROIs containing veins perpendicular to B_0 and ROIs of surrounding tissue, we estimated the contrast in dependence of TE.

Phase images were created by reconstructing the phase images for each coil individually for the high resolution transverse dataset. Using the 2D unwrapping tool Φ UN [17–19],

these images were unwrapped while masking out regions of low SNR. The eight resulting volumes were high-pass filtered and averaged using weighting factors: for each coil a smoothed magnitude image using a large kernel was created while disregarding information coming from outside the brain to avoid brain edge enhancement. These images were used as estimated sensitivity profiles. For each voxel, a coil's weighting factor was calculated as the intensity of the voxel in the smoothed image of that coil divided by the sum over all coils.

MR venography

The performance of two automated vein segmentation methods (described below) was evaluated in a low and high SNR situation using the magnitude of a functional SWI dataset of the occipital cortex where it was important to automatically identify veins. Due to the nature of the coil, a large signal intensity gradient was present (see Fig. 1a depicting the slab orientation and Fig. 1b showing a central slice of the dataset). Because a part of both vein segmentation filters was sensitive to absolute intensity values, this inhomogeneity gradient was corrected for by estimating a low frequency bias field. This bias field was obtained by smoothing the magnitude data with a very large (20 mm FWHM) Gaussian kernel while ignoring the data outside the brain to avoid edge enhancement. To test performance in a high SNR case an average over four volumes after motion correction was used, for the low SNR case a single volume was taken. Motion correction was performed using a weighting volume, because the fat on the scalp would otherwise severely compromise the motion parameter estimation due to its movement with respect to the brain.

Further processing was performed using the vesselness filter developed by Frangi et al. [20] at the Image Sciences Institute Utrecht (dubbed Utrecht vesselness filter further on) and by using vessel enhancing diffusion (VED) [21]. In the following we briefly describe these methods, a more detailed description can be found in [21]. In addition, manual vein segmentation was performed on the average volume to be compared with the automated segmentation approaches. Apart from assessing the performance of both filters with respect to SNR in the case of a functional experiment, using a dedicated coil covering the visual cortex only, we also applied both filters to a whole brain dataset acquired at 3 T and applied the VED filter to a whole brain dataset of the same subject acquired at 7 T.

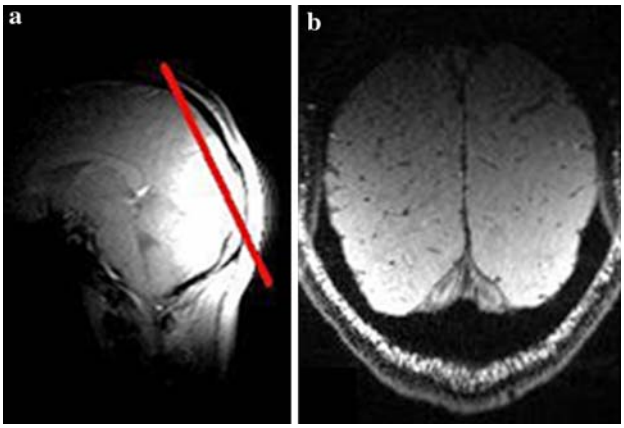

Fig. 1 Overview of occipital SWI dataset showing the extent of intensity inhomogeneity; **a** approximate slab orientation, **b** magnitude image of a single slice of this 3D dataset. 49 × 35 mm (150 × 150 DPI)

Vesselness filter

The Utrecht vesselness filter is based on the second order image information, represented by the Hessian matrix. By analysing the eigensystem of the Hessian, a likeliness function can be formulated to distinguish tubular structures (vessels) from non-tubular structures (e.g., background noise). The Hessian is calculated at a particular spatial scale which will be varied to detect vessels of different diameters. The eigenvalues (λ_j) of the Hessian, sorted by increasing magnitude ($|\lambda_1| < |\lambda_2| < |\lambda_3|$), describe the local second order structure in an image. For instance, if λ_3 has a high value and λ_1 and λ_2 are low, it means that there is an intensity change in a single direction only, in other words, we are dealing with a plate-like structure. The vesselness filter function is constructed to respond to dark tubular structures and to suppress all other structures by using these eigenvalues and three tuning parameters: one suppressing blob-like structures (α), one suppressing plate-like structures (β) and one suppressing background noise (c). This last one is sensitive to the absolute intensity of the image. The total vessel-likeliness filter which selects vessels which are dark with respect to their surroundings is shown in Eq. 2.

$V = 0$ in case $\lambda_1 > 0$ or $\lambda_2 > 0$, else

$$V = \left(1 - e^{-\frac{R_A^2}{2\alpha^2}}\right)\left(e^{-\frac{R_B^2}{2\beta^2}}\right)\left(1 - e^{-\frac{S^2}{2c^2}}\right) \tag{2}$$

with

$$R_A = \frac{(\text{Largest Cross Section Area})/\pi}{(\text{Largest Axis Semi-length})^2} = \frac{|\lambda_2|}{|\lambda_3|} \tag{3}$$

$$R_B = \frac{\text{Volume}/(4\pi/3)}{(\text{Largest Cross Section Area}/\pi)^{3/2}} = \frac{|\lambda_1|}{\sqrt{|\lambda_2\lambda_3|}} \tag{4}$$

$$S = \|H\|_F = \sqrt{\sum_{j \le D} \lambda_j^2}. \tag{5}$$

In this study, the values for α and β were both 0.5 as suggested in [20]. In previous work [22] we investigated the influence of parameter c and found that a too low value will

degrade the contrast of the Utrecht filter output. A too high value will not affect this contrast, however it will lower the absolute value of the vessel likeliness which, in turn, degrades the performance of the VED filter (explained below) as it makes use of the Utrecht filter output. In the current study a good value for c was empirically found to be 10% of the median intensity value within the brain after inhomogeneity correction. The spatial scale of the filter was varied between 0.1 and 1 mm. Note that using a scale of 0.1 mm does not mean we can detect vessels of 0.1 mm in diameter, which is much smaller than the voxelsize. It just means that the standard deviation of the Gaussian used to calculate the derivatives is 0.1 mm, i.e., the derivative is calculated in an almost discrete fashion.

Vessel enhancing diffusion

The VED filter method [21] is an iterative process making use of the vesselness filter. During each iteration the data is processed in such a way that the vesselness filter output will be improved in the next iteration by applying a diffusion scheme of varying (an)isotropy to the data. The nature of this scheme is determined by the vessel-likeliness found by the vesselness filter. If the voxel in question has a low vessel-likeliness, isotropic diffusion occurs, if it has a high vessel-likeliness, anisotropic diffusion occurs *in the direction of the vessel*. The strength of the vessel-likeliness response is determined by separate parameters of the VED (in this study, $\omega = 25$, $\varepsilon = 0.01$ and $t = 0.001$, for further details on these parameters see [21]). After the dataset has been "smoothed" in this fashion, the vesselness filter is applied again to determine the new vessel-likeliness and the process is repeated a number of times. In this study five iterations were used.

Filter performance assessment

To assess the performance of both filters with respect to SNR, maximum intensity projections over a few (eleven) slices were made along with a minimum intensity projection of the same slices of the original data. The VED filter output was thresholded and overlaid onto the original data to be compared to an overlay image of the manual segmentation. Both overlays were based upon the high SNR case. For the whole brain datasets maximum intensity projections were made to qualitatively assess the differences between vesselness filtering only and VED at 3 T. The 3 T VED result was also compared to the 7 T result. Note that in order to obtain good 3D projections of the datasets the brain was extracted (i.e., the skull was removed) in every dataset using FSL–BET.

Results

T_2^* contrast at different field strengths

In our relaxation time measurements at 7 T, T_2^* values of 32.9 $\pm$ 2.3 ms (occipital GM), 27.7 $\pm$ 4.3 ms (occipital WM outside the optical tract), 7.4 $\pm$ 1.4 ms (venous blood within the sagittal sinus) were found which are in excellent agreement with literature values [23]. Literature values for T_2^* of gray and white matter as well as venous blood at common field strengths (1.5, 3, and 7 T) are given in Table 1. It becomes clear that the range of values is relatively large which may in part be attributed to the influence of macroscopic B_0 inhomogeneity. In order to estimate T_2^* related contrast, we make use of Eq. 1 and insert the field dependent T_2^* values. For simulations of the GE contrast between blood and tissue at different B_0, the mean T_2^* value of the range, given in Table 1, was used for 1.5 and 3 T. For 7 T the values obtained in this study were used. As GM and WM have very similar T_2^*, GM is assumed to be representative for brain tissue. Optimal T_2^* contrast can then be estimated to occur at an echo time of around 64 ms (1.5 T), 35 ms (3 T) and 14 ms (7 T). In Fig. 2 the contrast normalised to the GM signal at TE = 20 ms is plotted versus TE for the three field strengths. Compared to 1.5 T, the contrast at the echo time where the maximum contrast occurs (without accounting for noise) is increased by a factor of 2.7 at 3 T and 4.6 at 7 T, respectively. We compared these simulations to the measured contrast between veins perpendicular to B_0 and surrounding tissue at 7 T. These values are plotted as squares ($\pm$ standard deviation over subjects) in Fig. 2. The echo time where maximum contrast at 7 T occurs (i.e., at 15 ms) corresponds very well to the one found in the simulations. The normalised contrast was different due to additional dephasing effects that are not accounted for in the simulations. Accordingly, in all MR venography measurements an echo time of 15 ms was used to obtain optimum contrast for veins.

Table 1 T_2^* relaxation times (ms) of gray matter, white matter and venous blood as a function of magnetic field strength

T_2^* (ms)	1.5 T	3 T	7 T
Venous blood ($Y \sim 0.7$)	42[b]–70[a]	20–29[g]	6.8[c]–13[f]
Gray matter	65[d]–84[h]	41.6[e]–66[h]	33.2[h]–36[f]
White matter	66.2[h]	48.4[e]–53.2[h]	26.8[h]–35[f]

[a] Chien et al. [37]
[b] Barth and Moser [38]
[c] Yacoub et al. [39]
[d] Kruger et al. [40]
[e] Wansapura et al. [41]
[f] Li et al. [42]
[g] Blockley et al. [43]
[h] Peters et al. [23]

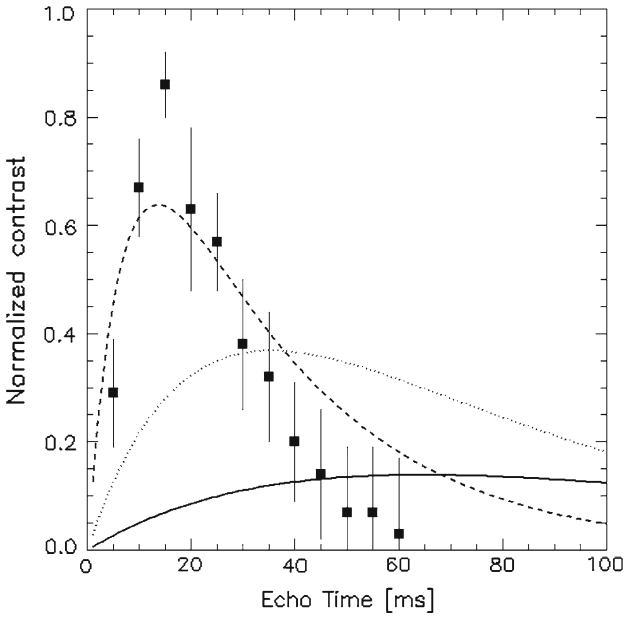

Fig. 2 Simulated T_2^* contrast between brain tissue and blood. Contrast is plotted versus TE for different B_0 (*solid line*: 1.5 T; *dotted line*: 3 T; *dashed line*: 7 T). Square symbols represent measured contrast between veins perpendicular to B_0 and surrounding tissue at 7 T, error bars reflect standard deviation over subjects. Contrast is normalised to the GM signal at TE = 20 ms. 129 × 129 mm (150 × 150 DPI)

In Fig. 3a magnitude and phase images of a high resolution, transverse SWI dataset acquired at 7 T using a TE of 15 ms is shown. To appreciate the small details zoomed sections of this dataset are shown in Fig. 3b. Note the high contrast even for very small anatomical structures visible on the zoomed magnitude and phase images, such as intracortical veins and layered structure of gray matter. Although generally the magnitude images show more details some structures are only visible on the phase images.

MR venography

Figure 4 shows the projection images of the filter results. Fig. 4a–c shows the mIP of the low SNR data (a), the MIP of its vesselness filter output (b) and the MIP of its VED filter output (c), respectively. In Fig. 4a the veins are clearly visible as dark structures within the bright brain tissue. The top part of the image (the more anterior–dorsal part) which is furthest away from the coil array suffers from very low SNR. In this region the vesselness filter (Fig. 4b) clearly fails to suppress the noise. The VED filter (Fig. 4c) is better able to contrast the vessels with respect to the noisy background although at extremely low SNR values it still shows a lot of false vein classification. Figure 4d–f shows the same as Fig. 4a–c for the higher SNR case. While the Utrecht vesselness filter (Fig. 4e) does not result in a good contrast between noise and vessels, the VED (Fig. 4f) shows good results. The result from Fig. 4f was compared to manual segmentation using two overlay images. Figure 4g shows the manual segmentation overlaid upon Fig. 4d, the mIP of the average dataset. Figure 4h shows the VED result from Fig. 4f overlaid on Fig. 4d. Apart from the uppermost part of the noisy region, the VED filter output is comparable to manual segmentation.

Figure 5 shows MR venograms of the whole brain scans of the same subject at 3 T (both Utrecht vesselness filter results as well as VED results are shown) and 7 T (VED results shown). Note the detailed depiction of the venous vasculature.

Discussion

Phase and T_2^* contrast at different field strengths

In addition to the contrast based on T_2^* effects, the contrast is also influenced by a phase effect that is due to the bulk magnetic susceptibility within the venous vessel. This causes an average frequency shift for all the protons inside the vessel. The accumulated phase angle Φ of the venous blood can be written as [24]

$$\phi(TE) = \gamma \cdot \Delta B \cdot TE \tag{6}$$

where γ is the magnetogyric ratio for protons (2.678×10^8 rad/sT), ΔB the field difference between blood and surrounding tissue. In a simple approach the magnetic field ΔB inside the vessel can be written as

$$\Delta B = 2 \cdot \pi \cdot \chi_{do} \cdot B_0 \cdot \left(\cos^2\theta - \frac{1}{3}\right) \cdot (1 - Y) \cdot \mathrm{Hct} \tag{7}$$

where χ_{do} is the susceptibility difference between fully deoxygenated and fully oxygenated blood, Y is the fractional oxygen saturation of the blood in the vessel, and Hct is the average volume fraction of hematocrit in blood. θ represents the angle between the blood vessel and the static field, B_0. In case $\theta = 0°$ one can estimate the maximum dephasing between vein and tissue if both are present within a voxel. Setting the parameters accordingly to $Y = 0.7$ [25], Hct = 0.40 [26], χ_{do} to 0.27×10^{-6} [27], this yields $\Phi \approx 12 \cdot \pi \cdot TE \cdot B_0$. The maximum signal cancellation—i.e., phase difference Φ equal to π, between tissue and a vein that runs parallel to B_0 should then occur at TE equal 57 ms (1.5 T), 28 ms (3 T), and 12 ms (7 T). In case $\theta \neq 0°$ an additional extravascular field around the vessel will cause additional dephasing that is quite complex and also depends on vessel size, vessel position and the ratio of voxel dimensions [28]. These parameters also influence the signal decay versus TE. However, an in vivo study has shown that a signal minimum (i.e., maximum contrast) occurs at a comparable TE for both the parallel case as well as the other extreme case when the vessel runs perpendicular to B_0 [29].

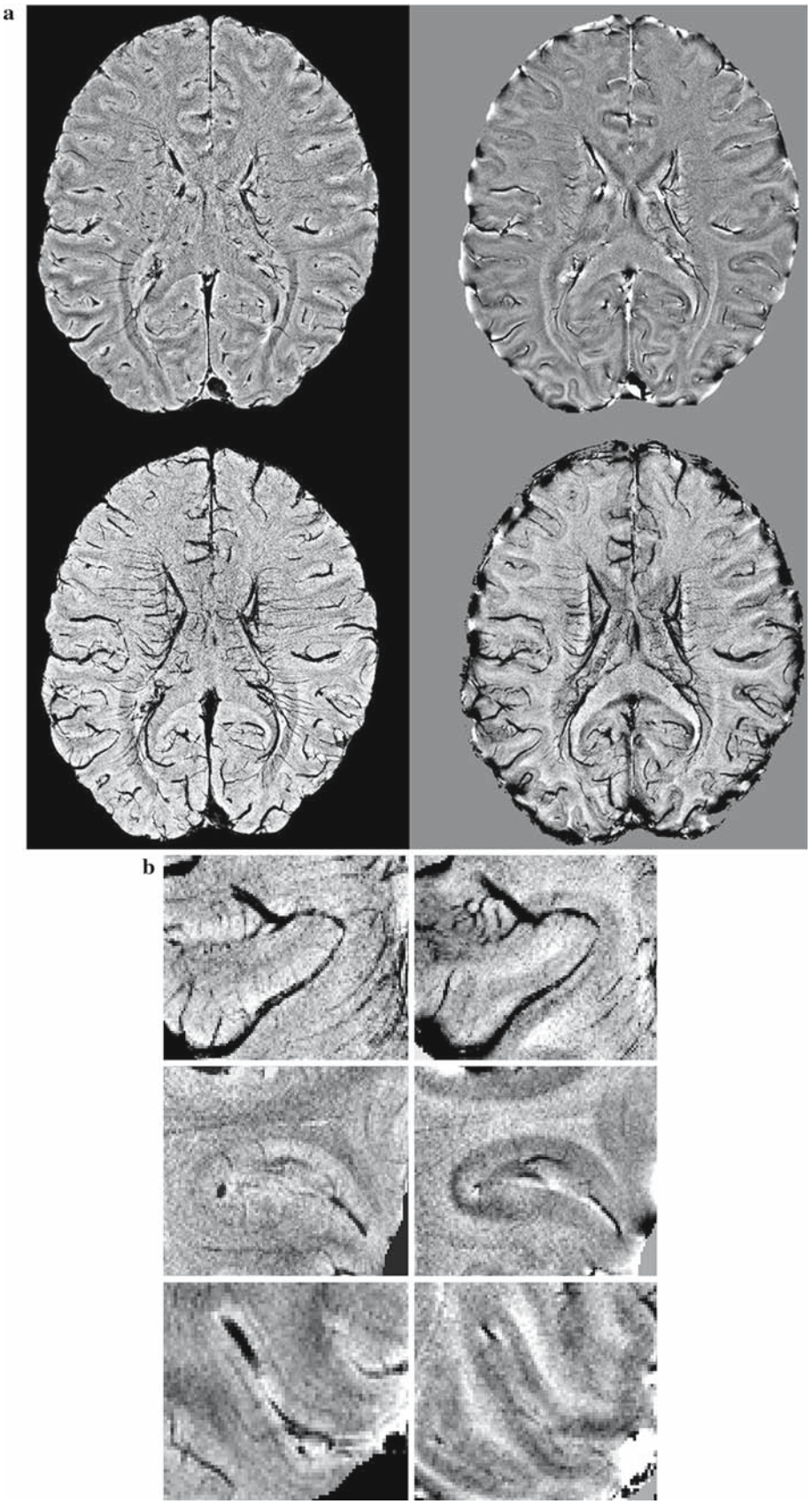

Fig. 3 **a** Magnitude (*left column*) and corresponding phase image (*right column*) of an SWI dataset acquired at 7 T (*top row* single slice; *bottom row* mIP over five slices). 199 × 213 mm (150 × 150DPI) **b** Zoomed sections of the dataset shown in Fig. 3a, magnitude (*left column*) and corresponding phase images (*right column*). *First row* shows the mIP of five slices, second row shows intracortical veins, *bottom row* shows stripe of Gennari. Note the high contrast even for very small anatomical structures visible on the zoomed magnitude and phase images, such as intracortical veins and layered structure of gray matter. Although generally the magnitude images show more details some structures are only visible on the phase images (see e.g., *top row* mIP). 151 × 178 mm (150 × 150 DPI)

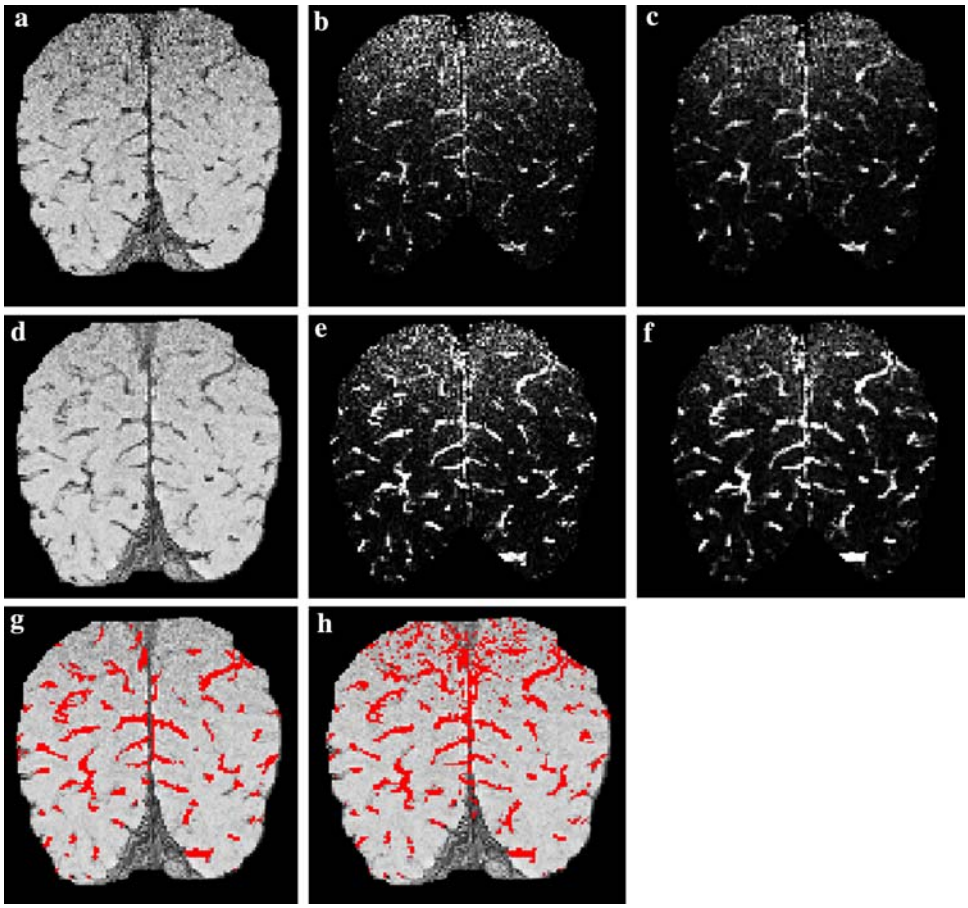

Fig. 4 Vessel segmentation results; *top row* is low SNR case, *middle row* is high SNR case. mIPs over 11 slices of the original data are shown in **a** and **d**. Utrecht vesselness filter results are shown as MIPs in **b** and **e**. VED MIPs are shown in **c** and **f**. Manual segmentation overlaid on **d** is shown in **g**. VED segmentation (**f**) is overlaid on **d** shown in **h**. 133 × 133 mm (150 × 150 DPI)

One also has to keep in mind that while the phase images show a very nice contrast between gray matter and white matter, the purpose of our study was to optimise the contrast between veins and tissue and not between GM and WM.

In contrast to previously published high resolution data at 7 T [30], our data were acquired using a 3D sequence which is $\sqrt{N_{\mathrm{SLICES}}}$ more efficient than the equivalent 2D sequence. This, and the usage of an acceleration factor of two, allowed us to acquire 72–128 slices in less than 15 min, either to cover the whole brain or to obtain a very high spatial resolution. Especially at 7 T, ghosting can lead to significant artefacts due to breathing. These were found to be either negligible due to the low signal intensity of the ghosts compared to the high signal within the brain in case of the whole brain acquisition or they could be prevented by simply using a phase correction based upon a navigator echo. However, high fields have several disadvantages that can be challenging. In our study, severe susceptibility artefacts in magnitude images could be minimised by using very high resolution, and the increased phase wraps in the phase images could be dealt with by unwrapping the single coil images and proper combination as proposed in the materials and methods section. However, the lower SNR in certain regions of the brain due to B_1 inhomogeneities leads to a reduced performance of the vessel filters. This can be seen by comparing the whole brain venograms at 3 T with those acquired at 7 T, but one has to keep in mind that the datasets at 7 T were acquired in much shorter time than those at 3 T.

MR venography

MR venography based on SWI has often used minimum intensity projections (mIP) to show the connecting vascular tree. While this works very well in case of near transverse slice positioning (see Fig. 3) in regions where the diameter and shape of the brain does not change significantly between slices, this can be problematic in other situations. mIPs also cannot be used for vessel classification. To solve this it has been proposed to use vesselness filters known from angiography [31]. We showed in this study that VED filtering outperforms a vesselness filter alone in regions of low SNR, suppressing more noise while leaving the underlying veins intact. The advantage of using a diffusion filter in addition to a vesselness filter is that it gets rid of false positives (typically noise) and that it restores suppressed connections, where thresholding after application of the vesselness filter is too rigid [22]. Note, that in all result images a brain mask is applied. This is necessary because the skull, the sagittal

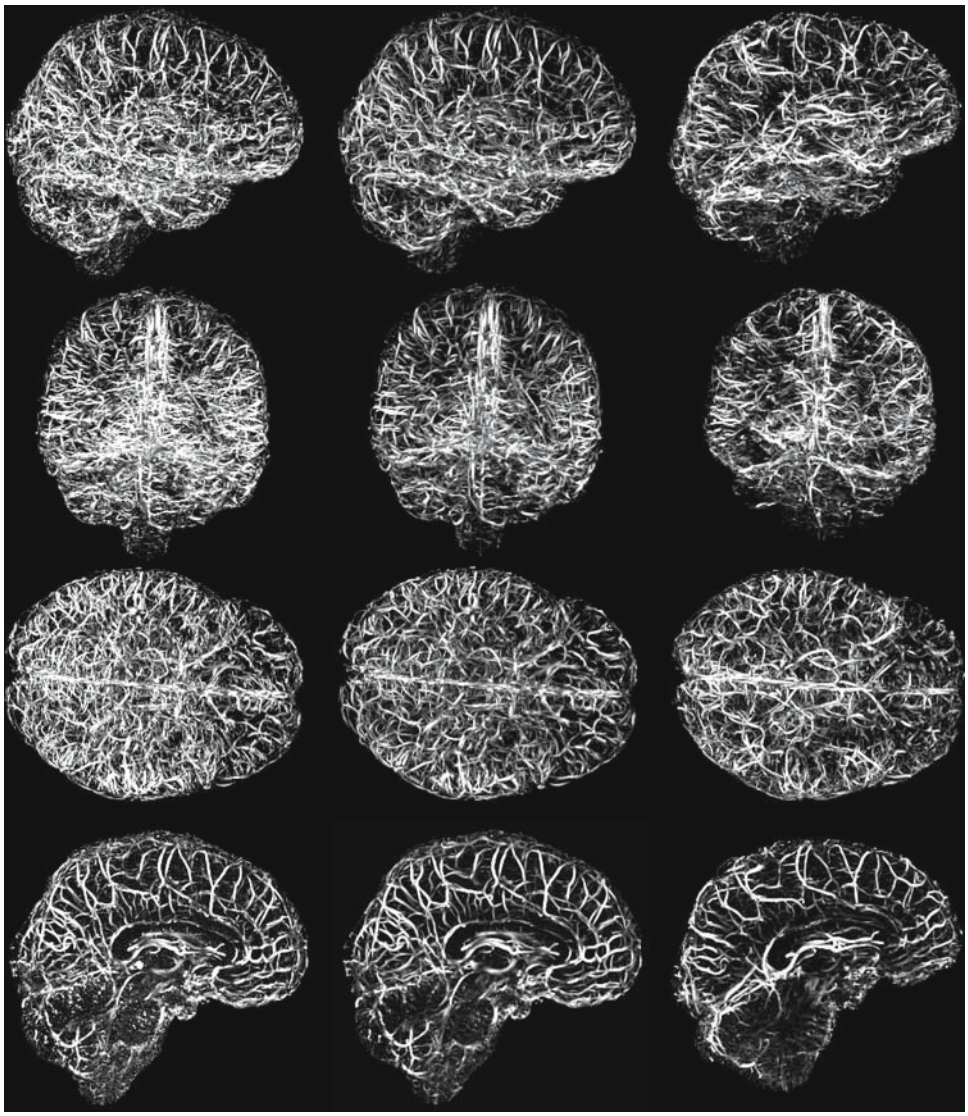

Fig. 5 Whole brain MR venograms using datasets acquired at 3 T using the Utrecht vesselness filter (*first column*) and 5 iterations of the VED (*second column*). The *third column* shows the VED filtered dataset of the same volunteer acquired at 7 T. *Rows* show MIPs of sagittal, coronal, and transverse orientation, as well as of several slices along the *midline*, respectively. 330 × 376 mm (150 × 150 DPI)

sinus and other surrounding structures/tissue would compromise the projection images. Another reason is that the Utrecht vesselness filter seems to have problems to fully suppress the sharp boundary at the pial surface, a notion previously reported in [31] as well. The results obtained from the VED method are good and comparable to manual segmentation results. This allows for segmentation of veins in a whole brain dataset where laborious manual segmentation is highly undesirable.

In SWI reconstruction [1] magnitude data are multiplied by a phase mask. This phase mask is an image in which all positive phase values are put to one and all negative phase values are put between zero and one according to a user-defined relation. At the lower field strength of 1.5 T, this combination was especially important as it enhanced the contrast of veins. However, at higher field strengths, the phase image has become an important source of information of its own right [6,32] giving insight into the iron metabolism [33,34] and into cortical substructures such as cortical layers [30,35] that can be visualised with very high detail at 7 T. This causes the phase image to become quite difficult to interpret, due to its dependence on shape of the object of interests (e.g., vessel, cortical ribbon, deep brain nucleus) and due to the background field inhomogeneities that have to be filtered out. The consequence is that SWI reconstruction can become problematic as next to veins, other sources of negative phase values like tissue boundaries will be enhanced as well. As, to our knowledge, the optimal phase mask relationship to enhance veins only has not been determined yet, we chose to use only the magnitude data to assess the vessel filters. We do believe however that the phase information could improve venography results once the methods to exploit this information have been developed. Please note that the magnitude data is affected by phase effects: partial voluming of blood and tissue within a voxel causes both a phase shift (phase image) and signal cancellation due to dephasing (magnitude

image). As shown in animal studies at high field strength, the magnitude alone gives magnificent intracortical details of the vasculature of the brain [35,36].

Conclusion

Based on simulations performed in our study, vein–tissue contrast is higher at higher fields at a shorter TE due to the shorter T_2^* relaxation time of venous blood and faster dephasing between venous blood and tissue. When using an optimum echo time tiny intracortical veins could be detected in the SWI datasets acquired at 7 T in a short measurement time. We also showed the feasibility of constructing detailed whole brain MR venograms by application of a vessel enhancing diffusion filter.

Acknowledgments We thank Benedikt Poser for his support with the measurements at 7 T, and him and David Norris for critically reading the manuscript. This work was supported by NWO grant ALW2PJ/04064 and FWF grant J2439-B02.

References

1. Haacke EM, Xu Y, Cheng YC, Reichenbach JR (2004) Susceptibility weighted imaging (SWI). Magn Reson Med 52(3): 612–618
2. Ogawa S, Lee TM, Nayak AS, Glynn P (1990) Oxygenation-sensitive contrast in magnetic resonance image of rodent brain at high magnetic fields. Magn Reson Med 14(1):68–78
3. Reichenbach JR, Essig M, Haacke EM, Lee BC, Przetak C, Kaiser WA, Schad LR (1998) High-resolution venography of the brain using magnetic resonance imaging. Magn Reson Mater Phys (MAGMA) 6(1):62–69
4. Reichenbach JR, Haacke EM (2001) High-resolution BOLD venographic imaging: a window into brain function. NMR Biomed 14(7–8):453–467
5. Reichenbach JR, Venkatesan R, Schillinger DJ, Kido DK, Haacke EM (1997) Small vessels in the human brain: MR venography with deoxyhemoglobin as an intrinsic contrast agent. Radiology 204(1):272–277
6. Barth M, Nobauer-Huhmann IM, Reichenbach JR, Mlynarik V, Schoggl A, Matula C, Trattnig S (2003) High-resolution three-dimensional contrast-enhanced blood oxygenation level-dependent magnetic resonance venography of brain tumors at 3 Tesla: first clinical experience and comparison with 1.5 Tesla. Invest Radiol 38(7):409–414
7. Rauscher A, Sedlacik J, Fitzek C, Walter B, Hochstetter A, Kalff R, Kaiser WA, Reichenbach JR (2005) High resolution susceptibility weighted MR-imaging of brain tumors during the application of a gaseous agent. Rofo 177(8):1065–1069
8. Sehgal V, Delproposto Z, Haddar D, Haacke EM, Sloan AE, Zamorano LJ, Barger G, Hu J, Xu Y, Prabhakaran KP, Elangovan IR, Neelavalli J, Reichenbach JR (2006) Susceptibility-weighted imaging to visualize blood products and improve tumor contrast in the study of brain masses. J Magn Reson Imaging 24(1):41–51
9. Noebauer-Huhmann IM, Pinker K, Barth M, Mlynarik V, Ba-Ssalamah A, Saringer WF, Weber M, Benesch T, Witoszynskyj S, Rauscher A, Reichenbach JR, Trattnig S (2006) Contrast-enhanced, high-resolution, susceptibility-weighted magnetic resonance imaging of the brain: dose-dependent optimization at 3 tesla and 1.5 tesla in healthy volunteers. Invest Radiol 41(3):249–255
10. Tong KA, Ashwal S, Holshouser BA, Shutter LA, Herigault G, Haacke EM, Kido DK (2003) Hemorrhagic shearing lesions in children and adolescents with posttraumatic diffuse axonal injury: improved detection and initial results. Radiology 227(2):332–339
11. Hermier M, Nighoghossian N (2004) Contribution of susceptibility-weighted imaging to acute stroke assessment. Stroke 35(8): 1989–1994
12. Tan IL, van Schijndel RA, Pouwels PJ, van Walderveen MA, Reichenbach JR, Manoliu RA, Barkhof F (2000) MR venography of multiple sclerosis. AJNR Am J Neuroradiol 21(6):1039–1042
13. Barth M, Norris DG (2007) Very high-resolution three-dimensional functional MRI of the human visual cortex with elimination of large venous vessels. NMR Biomed 20(5):477–484
14. Wiesinger F, Van de Moortele PF, Adriany G, De Zanche N, Ugurbil K, Pruessmann KP (2006) Potential and feasibility of parallel MRI at high field. NMR Biomed 19(3):368–378
15. Yablonskiy DA, Haacke EM (1994) Theory of NMR signal behavior in magnetically inhomogeneous tissues: the static dephasing regime. Magn Reson Med 32(6):749–763
16. Griswold MA, Jakob PM, Heidemann RM, Nittka M, Jellus V, Wang J, Kiefer B, Haase A (2002) Generalized autocalibrating partially parallel acquisitions (GRAPPA). Magn Reson Med 47(6):1202–1210
17. Rauscher A, Barth M, Reichenbach JR, Stollberger R, Moser E (2003) Automated unwrapping of MR phase images applied to BOLD MR-venography at 3 Tesla. J Magn Reson Imaging 18(2):175–180
18. Witoszynskyj S, Rauscher A, Reichenbach JR, Barth M (2005) Automated phase unwrapping of MR images at different field strengths using multiple quality maps. In: Proceedings of the ISMRM, p 2249
19. Witoszynskyj S, Rauscher A, Reichenbach JR, Barth M (2007) Φ UN (Φ ase UNwrapping)—validation of a 2D region-growing phase unwrapping program. In: Proceedings of the ISMRM, p 3436
20. Frangi AF, Niessen WJ, Vincken KL, Viergever MA (1998) Multiscale vessel enhancement filtering. In: Wells WM (ed) III ACF-CaSD, LNCS, pp 130–137
21. Manniesing R, Viergever MA, Niessen WJ (2006) Vessel enhancing diffusion—a scale space representation of vessel structures. Med Image Anal 10(6):815–825
22. Koopmans PJ, Manniesing R, Norris DG, Viergever M, Niessen WJ, Barth M (2006) Vein segmentation from 3D high resolution MR venograms by using vessel enhancing diffusion. European Society for Magnetic Resonance in Medicine and Biology, Warsaw, p 361
23. Peters AM, Brookes MJ, Hoogenraad FG, Gowland PA, Francis ST, Morris PG, Bowtell R (2007) T(2)* measurements in human brain at 1.5, 3 and 7 T. Magn Reson Imaging 25(6):748–753
24. Reichenbach JR, Barth M, Haacke EM, Klarhofer M, Kaiser WA, Moser E (2000) High-resolution MR venography at 3.0 Tesla. J Comput Assist Tomogr 24(6):949–957
25. Haacke EM, Lai S, Yablonskiy DA, Lin W (1995) In vivo validation of the BOLD mechanism: a review of signal changes in gradient echo functional MRI in the presence of flow. Int J Imaging Syst Technol 6:153–163
26. Pawlik G, Rackl A, Bing RJ (1981) Quantitative capillary topography and blood flow in the cerebral cortex of cats: an in vivo microscopic study. Brain Res 208(1):35–58
27. Spees WM, Yablonskiy DA, Oswood MC, Ackerman JJ (2001) Water proton MR properties of human blood at 1.5 Tesla: magnetic susceptibility, T(1), T(2), T*(2), and non-Lorentzian signal behavior. Magn Reson Med 45(4):533–542
28. Xu Y, Haacke EM (2006) The role of voxel aspect ratio in determining apparent vascular phase behavior in susceptibility weighted imaging. Magn Reson Imaging 24(2):155–160

29. Sedlacik J, Rauscher A, Reichenbach JR (2007) Obtaining Blood Oxygenation Levels from MR Signal Behaviour in the Presence of Single Venous Vessels. Magn Reson Med 58(5):1035–44
30. Duyn JH, van Gelderen P, Li TQ, de Zwart JA, Koretsky AP, Fukunaga M (2007) High-field MRI of brain cortical substructure based on signal phase. Proc Natl Acad Sci USA 104:11796–11801
31. Deistung A, Kocinski M, Szczypinski P, Materka A, Reichenbach JR (2006) Segmentation of venous vessels using multi-scale vessel enhancement filtering in susceptibility weighted imaging. In: Proceedings of the ISMRM, ISMRM, Seattle, p 1948
32. Rauscher A, Sedlacik J, Barth M, Mentzel HJ, Reichenbach JR (2005) Magnetic susceptibility-weighted MR phase imaging of the human brain. AJNR Am J Neuroradiol 26(4):736–742
33. Haacke EM, Cheng NY, House MJ, Liu Q, Neelavalli J, Ogg RJ, Khan A, Ayaz M, Kirsch W, Obenaus A (2005) Imaging iron stores in the brain using magnetic resonance imaging. Magn Reson Imaging 23(1):1–25
34. Ogg RJ, Langston JW, Haacke EM, Steen RG, Taylor JS (1999) The correlation between phase shifts in gradient-echo MR images and regional brain iron concentration. Magn Reson Imaging 17(8):1141–1148
35. Bolan PJ, Yacoub E, Garwood M, Ugurbil K, Harel N (2006) In vivo micro-MRI of intracortical neurovasculature. Neuroimage 32(1):62–69
36. Pfeuffer J, Merkle H, Beyerlein M, Steudel T, Logothetis NK (2004) Anatomical and functional MR imaging in the macaque monkey using a vertical large-bore 7 Tesla setup. Magn Reson Imaging 22(10):1343–1359
37. Chien D, Levin DL, Anderson CM (1994) MR gradient echo imaging of intravascular blood oxygenation: T_2^* determination in the presence of flow. Magn Reson Med 32(4):540–545
38. Barth M, Moser E (1997) Proton NMR relaxation times of human blood samples at 1.5 T and implications for functional MRI. Cell Mol Biol 43(5):783–791
39. Yacoub E, Shmuel A, Pfeuffer J, VanDe Moortele PF, Adriany G, Andersen P, Vaughan JT, Merkle H, Ugurbil K, Hu X (2001) Imaging brain function in humans at 7 Tesla. Magn Reson Med 45(4):588–594
40. Kruger G, Kastrup A, Glover GH (2001) Neuroimaging at 1.5 T and 3.0 T: comparison of oxygenation-sensitive magnetic resonance imaging. Magn Reson Med 45(4):595–604
41. Wansapura JP, Holland SK, Dunn RS, Ball WS Jr (1999) NMR relaxation times in the human brain at 3.0 T. J Magn Reson Imaging 9(4):531–538
42. Li TQ, van Gelderen P, Merkle H, Talagala L, Koretsky AP, Duyn J (2006) Extensive heterogeneity in white matter intensity in high-resolution T2*-weighted MRI of the human brain at 7.0 T. Neuroimage 32(3):1032–1040
43. Blockley NP, Francis ST, Gowland PA (2006) Dependence of R2* on oxygenation and contrast agent concentration in human blood at 3 T. In: Proceedings of the ISMRM, Seattle, p 2516